First-principle simulations of inorganic halides Li_2TlBiY_6 (Y = Cl, Br, I) for optoelectronic applications

N. A. Noor[a,*], F. Nasrullah[a], U. Afzaal[a], S. Mumtaz[b], M. Imran[c], I. M. Moussa[d]

[a]*Department of Physics, Riphah International University, Lahore Campus, 54000, Pakistan*

[b]*Department of Electrical and Biological Physics, Kwangwoon University, Seoul 01897, South Korea.*

[c]*Department of Electronics, Government College University, Lahore, Pakistan*

[d]*Department of Botany and Microbiology, College of Science, King Saud University, P.O. Box 2455, Riyadh, 11451, Saudi Arabia*

In this emerging technological era, lead-free (Li-based) inorganic halides have drawn a lot of researchers' consideration due to their optoelectronic applications. Based on this, we explored theoretically mechanical, optical, and thermoelectric features of halides Li_2TlBiY_6 (Y = Cl, Br, I) by employing first-principle simulations (Wien2k code). Our finding of optoelectronic parameters using appropriate mBJ approach is in favorable alignment to previously reported data, and PBEsol is employed to scrutinize structural as well as mechanical features of these materials. The Born stability and formation energy are examined concerning the structural stability associated with all halides. The distinction between brittle and ductile nature is investigated concerning the calculation of elastic constants of the cubic symmetry. Being based on the mBJ potential, the bandgasps for $Li_2TlBiCl_6$, $Li_2TlBiBr_6$, and Li_2TlBiI_6 are 2.8 eV, 2.3 eV, and 1.9 eV, correspondingly. To confirm their optimal absorbability in the electromagnetic domain (visible), all halides were further analyzed concerning dielectric parameters. Additionally, thermoelectric properties are explained in detail within the temperature range of 300-800K using classical Boltzmann theory, making them promising materials for thermoelectric applications.

(Received February 5, 2024; Accepted April 29, 2024)

Keywords: First-principle simulations, Inorganic halides, Mechanical properties, Direct bandgap, Optoelectronic application, Power factor

1. Introduction

For more than six decades, an interesting class of quaternary semiconductors has been the subject of in-depth research, which is termed halide double perovskites (DPs) or elpasolites. They have a standard composition of $A_2M^IM^{III}X_6$. This specific range of compounds drew more attention as the semiconductor $Cs_2AgBiBr_6$ is proposed to be an intriguing alternative material by the halide DPs community owing to its less toxicity in comparison to thoroughly investigated halides like $MAPbI_3$ (MA = methylammonium) or $CsPbBr_3$ [1-3]. In addition to this, Halide DPs prevail over traditional lead halide perovskites in terms of stability, which is favorable for meeting the potent situation of this era [4]. In this context, it is anticipated that solar cell technological innovation is extremely economical and effective in comparison to other renewable energy sources. Therefore, doing scientific research to investigate such affordable, durable, and effective cells requires an intense curiosity. However, moisture lowers the efficiency of inexpensive perovskites as solar cells [5, 6]. These are not the only reasons to oppose their profitability. Lead-based compounds' unstable and toxic nature are two of these causes [7]. However, a particular feature of these compounds that makes them valuable in photovoltaic technology is their ability to absorb light in the visible spectrum [8].

* Corresponding author: naveedcssp@gmail.com
https://doi.org/10.15251/DJNB.2024.192.679

Double perovskites are believed to be thermally and structurally stable, remarkably proficient, environmentally benign, and non-toxic in the last couple of decades. Besides these, compounds' electrical, optical, and transport properties are studied [9-12]. Nevertheless, the toxicity resulting from lead limitations and instability of organic modules restricts their commercial employment of compound (22.1%) more effectively [13]. the investigation of Pb-free perovskites, including $CsSnI_3$ and $CsGeI_3$, has figured out this problem. $CsSnI_3$ solar cells are susceptible to instability along with high performance of 13% [14]. On the other hand, DPs, $Y_2AgTlCl_6$ (Y = Rb, Cs), well investigated recently [15]. Rb_2TeX_6 (X = I, Br, Cl), are reported to be the best absorbent with remarkable stability [16, 17]. To mitigate our dependency on fossil fuels and maintain a clean environment, lead-free compound production is of utmost importance [18-20]. However, an enormous amount of research has also been done on hybrid perovskite molecules, which are a combo of organic and inorganic elements. like $CH_3NH_3PbX_3$ (where X = Cl, Br, and I), DP's remain portable as well as readily produced, but their reduced stability and toxicity provide a significant barrier to their application in photovoltaic devices [21]. Consequently, lead-free DPs have become a key concern in both theoretical and experimental research these days.

The potential significance features incorporate an immense rise in optical absorption along with a smaller bandgap in these particular compounds as compared to ordinary perovskites. Meanwhile, the performance of the solar collector can be raised by regulating the flow rate following adjustments in the concentration ratio, which is reported by Faddouli et al. [22]. Improvements in the solar cell efficiency of perovskite materials are predominantly lead-reliant. Therefore, to maintain the stability and effectiveness of perovskite structures, any possible substitute for lead must meet stringent standards [23]. One recent advancement is the use of the cation transmutation method to produce quaternary halides with a double perovskite structure. Two Pb^{2+} ions may be efficiently transformed via this process into a single monovalent and trivalent cation [24]. It ought to be noted that only trivalent bismuth (Bi^{3+}) and lead have the same electrical configuration among the core group elements. Researchers accomplished the synthesis of Bi-based halide double perovskites known as Cs_2AgBiX_6. These materials highlighted amazing properties including outstanding durability and a long carrier recombination lifespan. These characteristics make them a captivating choice in solar energy and photon sensing devices [25]. However, as reference [26] points out, the large band gap in Cs_2AgBiX_6 hinders the device's functionality. As such, it is imperative to develop a robust technique for precisely adjusting the band gaps of Cs_2AgBiX_6 and to obtain a profound understanding of the complex interaction among its composition and characteristics [27, 28].

Motivated by the above literature on DPs, we explored theoretically Li_2TlBiY_6 (Y = Cl, Br, I) halide DPs' structural, elastic, optoelectronic and thermal features to identify their possible applications in photovoltaic systems as well as thermoelectric devices.

2. Method of calculations

For structural, elastic as well as optoelectronic features of Li_2TlBiY_6 (Y = Cl, Br, I), we used Wien2k [29] oriented FP-LAPW+lo approach. To obtain ground state parameters, we performed optimization for DPs Li_2TlBiY_6 using generalized gradient approximation (GGA) [30]. This estimate captures the structural characteristics well, albeit the overestimation of the band gaps is shown. Thus, the energy band gaps have been rectified via TB-mBJ approach [31]. The LAPW+lo approach has been adopted for wave expansion in spheres, guaranteeing particle-like nature inside the spheres and wave-like performance outside. To determine the cut-off parameter, $R_{MT}\times Kmax$ was applied. For waves, the magnitude is 8, and for atomic nature, it is 10. In periodic boundary arrangement, the repetition of crystal structure is done by the application of the Brillion Zone (BZ) order. For assessing the physical and electrical features, likewise, for optical characteristics in BZ, a 4000-k point framework was used. Iterative cycles were constrained to produce energy variances under 10^{-4} Ry and charge variations beneath 10^{-3} e to get the convergence of energy and charge. In order to calculate transport characteristics, BoltzTrap coding

[32] was adopted, adding up to 4000 dense mesh k-points during the estimation process. The equations employed for the analysis of thermoelectric properties are given in Ref. [33, 34]:

3. Results and discussion

3.1. Structural and elastic properties

In DPs Li_2TlBiY_6 (Y = Cl, Br, I) structures, the space group (No. 225) has been tuned to remove strain forces inside atoms for a particular range related to structural limitations. The decline in atom-to-atom strain forces causes the structures to settle back to their expected positions. The calculated studied DPs structures are represented in ball format and polyhedrally in Fig. 1 (a, b), where two octahedra (TlY_6 and BiY_6) are populated with Li atoms and separated by 12 folds of Y atoms. The blue and pink hues in Figure 1 represent the Tl and Bi atoms, which are situated in the center of the octahedral crystal. The repetition of variant octahedra patterns is followed across the whole unit [35].

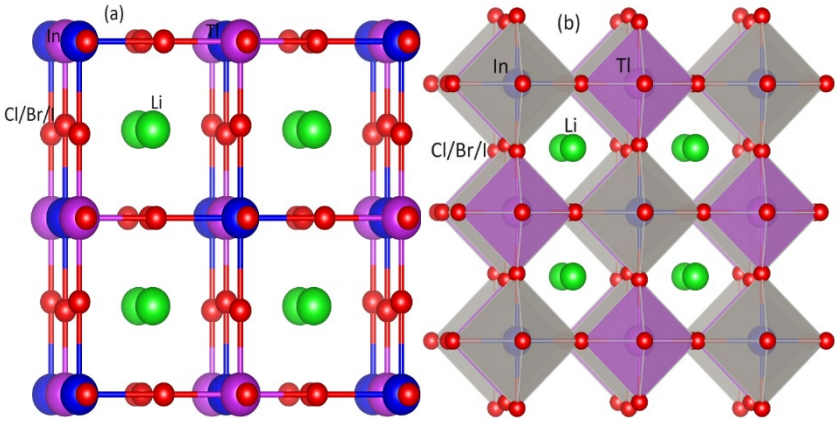

Fig. 1. Crystal structure plot of double perovskites Li_2TlBiY_6 (Y = Cl, Br, I) halides (a) ball format and (b) polyhedral format.

The substitution of Br and I atoms for Cl increases the magnitude of the lattice parameter (a_0). Raising the radius of ionic particles in an identical pattern is what caused it to occur [36]. Furthermore, a negative correlation between bulk modulus and lattice parameter has been noted, and this was fulfilled by the bulk modulus's decline [37]. To compute cubic lattice parameters (see Table 1), energy vs volume graphs tuned by PBEsol- GGA (see Fig. 2). Further, the thermal viability is authorized due to the computation of energy of formation with the mathematical expression [38]:

$$\Delta E_f = E_{\text{Total}}(\text{Li}_a Tl_b \text{Bi}_c \text{Y}_d) - aE_{\text{Li}} - bE_{\text{Tl}} - cE_{\text{Bi}} - dE_{\text{Y}} \quad (1)$$

Somehow the energies of individuals; Y, Tl, Bi, as well as Li are termed as E_{Y} , E_{Cu}, E_{Bi} and E_{Li} whereas the whole energy of the material is represented by $E_{\text{Total}}(\text{Li}_a Tl_b \text{Bi}_c \text{Y}_d)$. the ground state energies for respective atoms Tl, Bi, Li, and Y corresponding to the following composition $Li_2TlBiCl_6$, $Li_2TlBiBr_6$, and Li_2TlBiI_6 have been found in the process of optimization in order to calculate formation energy.

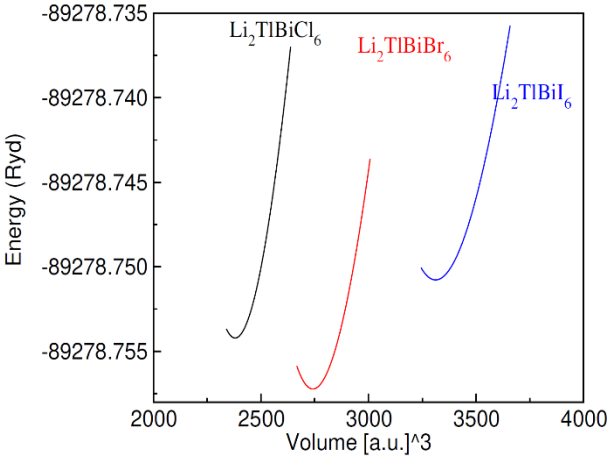

Fig. 2. Energy versus volume plot for $Li_2TlBiCl_6$, $Li_2TlBiBr_6$ and Li_2TlBiI_6 halides.

Materials deemed to be thermally durable, there will be a negative energy variation among whole energy of the complex as well as energy of each individual substituent. All of $Li_2TlBiCl_6$, $Li_2TlBiBr_6$, and Li_2TlBiI_6 DPs had negative formation energy values, which suggests thermodynamically stable (see Table 1).

Table 1. Computed figures of lattice parameter a_o(Å) in comparison with reported results, bulk modulus B_o(GPa), Enthalpy of formation (ΔH_f) and elastic parameters of Li_2TlBiY_6 (Y = Cl, Br, I) halides.

Parameters	$Li_2TlBiCl_6$	$Li_2TlBiBr_6$	Li_2TlBiI_6
	PBEsol-GGA	PBEsol-GGA	PBEsol-GGA
a_o(Å)	11.57	12.08	12.90
B_o (*GPa*)	22.10	18.58	14.87
ΔH_f (eV)	-2.18	-1.92	-1.62
C_{11}	55.06	46.65	36.80
C_{12}	6.04	4.09	3.22
C_{44}	3.07	2.22	1.15
B	22.38	18.27	14.41
G	8.18	6.65	4.61
Y	21.88	17.79	12.51
B/G	2.78	2.74	3.12
υ	0.33	0.34	0.35
A	0.13	0.10	0.07

The cubic structure compounds' mechanical and dynamic properties are connected by mechanical parameters (C_{11}, C_{12}, and C_{44}). A compound's ductile or brittle trait is validated by these moduli of elasticity values. The mechanical parameters found to be using the hook's law. Stability standards set average limits in respect of critical variables needed to assess the mechanical properties of the DPs. The following equation may be used to evaluate the mechanical integrity of cubic structures employing the Born-Huang durability criterion [39, 40]:

$$\begin{cases} C_{11} > 0 \\ C_{44} > 0 \\ C_{11} > C_{12} \\ C_{11} + 2C_{12} > 0 \end{cases} \quad (2)$$

On summarizing, one comes to know that the DPs in consideration being stable during elastic deformation since the elastic durability standards are validated. Furthermore, $C_{12} < B < C_{11}$ (refer to Table 1) moreover demonstrates the long-term integrity of the compounds. The hardness of the materials determined by their moduli of elasticity. Young's modulus illustrated that compound fracture is complex due to its higher value. $Li_2TlBiCl6$, $Li_2TlBiBr_6$, and Li_2TlBiI_6 are inflexible, but their higher Young's and Shear moduli are in line with the $Cs_2CdZnCl_6$ family of compounds [41]. The fracture resistance can be estimated by the Young's modulus (B), while the compounds' plastic deformation is assessed by the shear modulus (G). As the ratio computation resulted in value more than 1.75, the ductility of the compounds $Li_2TlBiCl_6$, $Li_2TlBiBr_6$, and Li_2TlBiI_6 surpasses the brittleness. As a result, as Table 1 illustrates, all are ductile. The range of μ parameter for solid materials (polymers, ceramics as well as metals) is 0.25 to 0.35 [42].

Nonetheless, in our investigated compounds, its acquired figure at 0 GPs is within the same range. As the results rises above 0.26, the compound ductile trait is considered. Because of its higher value, axial compression is found to be less than transversal expansion. An important factor in engineering science is the elastic anisotropy ($A = \frac{2C_{44}}{C_{11}-C_{12}}$), which establishes the kind of microcracks present in the materials being studied. For isotropic it value appear as 1 and for anisotropic their values deviate from one. Therefore, our calculated values deviate from 1, it mean all DPs are appear as anisotropic.

3.2. Electronic and optical properties

Energy bands as well as impact of changes in CB and VB are used to define the optoelectronic properties of DPs Li_2TlBiY_6. Estimating DOS and BS of a chemical is vital in assessing its optoelectronic characteristics. The BS and DOS of investigated DPs Li_2TlBiY_6, are illustrated in Figs. 3 and 4, correspondingly. Fig. 3 depicts, the band structure of DPs through investigation is ascertained using the mBJ estimations. The vacant Fermi level makes the composites' indirect semiconductor aspect evident. It has been demonstrated for wave-vector measurements for the two compounds that the VB maximum and CB minimum oriented in distinct alignments. $Li_2TlBiCl_6$, $Li_2TlBiBr_6$, as well as Li_2TlBiI_6 having calculated BGs of 2.8 eV, 2.3 eV, and 1.9 eV via the application of mBJ. Because all DPs are oppositely correlated to one another, the magnitude of the ionic radii had an impact on the BG magnitude (see Table 3). The value of BG falls in proportion to the size of ionic radii. The investigated compounds' indirect semiconducting behavior and BG values attest to their potential in the production of solar cell devices.

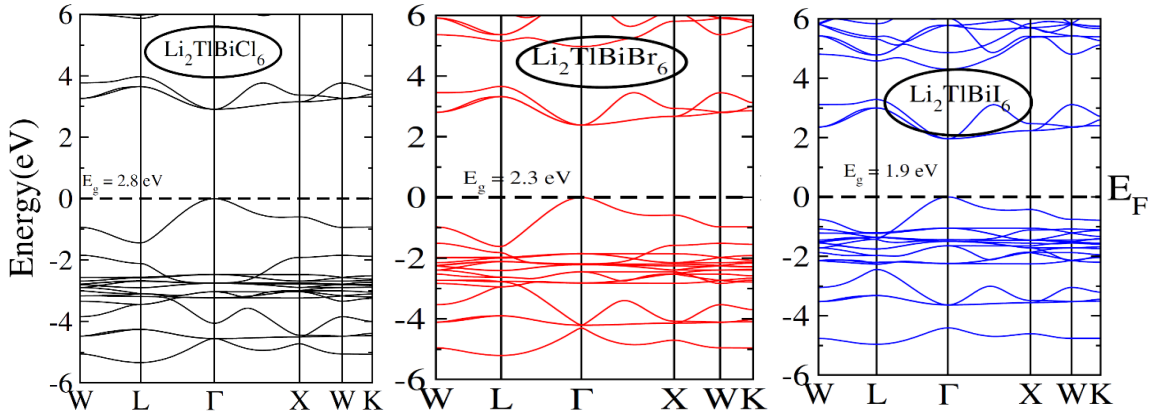

Fig. 3. Computed band structure for $Li_2TlBiCl_6$, $Li_2TlBiBr_6$ and Li_2TlBiI_6 halides.

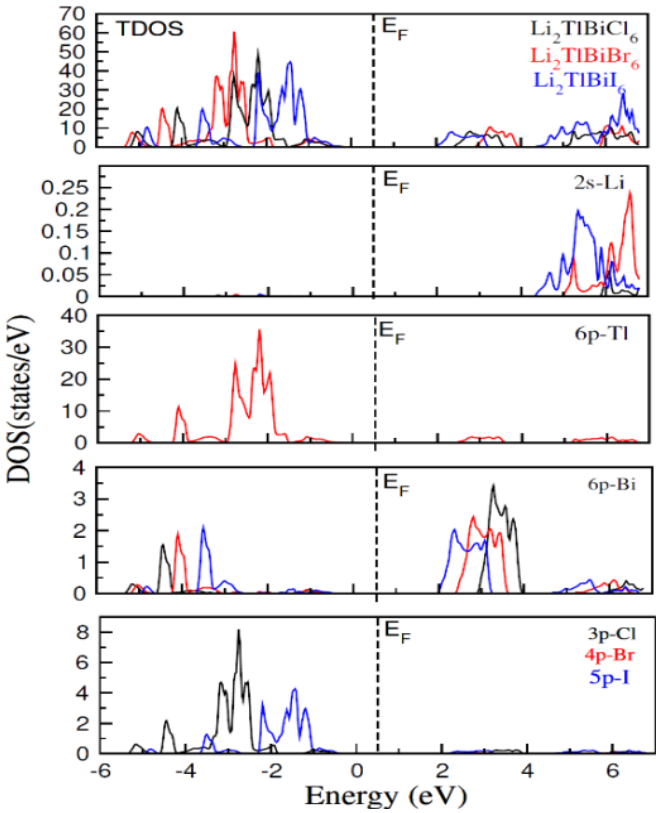

Fig. 4. Estimated TDOS along with PDOS $Li_2TlBiCl_6$, $Li_2TlBiBr_6$ and Li_2TlBiI_6 halides.

Figure 4 illustrates how the hybridization and electrical conversion from VB to CB are indicated by the PDOS and TDOS. Furthermore, Fig. 4 shows the valence states Y-p, Tl-6p, and Bi-6p that were supplied to the band configuration of Li_2TlBiY_6. Furthermore, Tl atoms in 6p-states that are near the Fermi level play a significant influence. In an analogous manner, Y p-states at a magnitude of -4.0 eV caused recombination in the VB to become noticeable. The movement of the E_F validates the presence of electron hole pair. However, at energy levels between 1 and 2 eV, in CB there is very little hybridization among Bi 6p orbital of and Li 2s orbitals.

The electrical and optical properties of the DP under examination are determined by its shift from VB to CB. Conversely, the hybridization of the states controls the gap and figures out the transition rate, significantly influencing the compound's optoelectronic features. Response of DPs Li_2TlBiZ_6(Z = Cl, Br, I) toward incoming radiations is explained via their opto-electronic features, emphasizing their role in solar cells production. The aforementioned properties mostly determined via carrier transitions, recombination rate, and the interaction of matter with light. This work ignores intraband shifts and focuses on the interband shifts of carriers. The recombination rate increases when matter and light collaborate, which is the only reason why electrons travel from VB to CB. $\varepsilon(\omega) = \varepsilon_1(\omega) + i\varepsilon_2(\omega)$, which has both dielectric properties is used to assess the optical properties of the compounds [43, 44]. The dielectric parameters of $\varepsilon(\omega)$ in Kramer-Kroning formula are listed as follows [45]:

$$\varepsilon_1(\omega) = 1 + \frac{2}{\pi} P \int_0^{\infty} \frac{\omega' \varepsilon_2(\omega')}{\omega'^2 - \omega^2} d\omega' \tag{3}$$

$$\varepsilon_2(\omega) = \frac{e^2 h\prime}{\pi m^2 \omega^2} \sum_{v,c} \int_{BZ} |M_{cv}(k)|^2 \delta[\omega_{cv}(k) - \omega] d^3k \tag{4}$$

thereby, the symbols for the angular frequency (ω), molar mass (M), principal quantum (P) and wave vector (k) are used, correspondingly. The dielectric components are investigated for calculating a variety of optical parameters. Fig. 5(a-f) shows these calculated factors for Li_2TlBiY_6 at the incoming energy level of 0 eV- 6 eV. Furthermore, the absorption of light is determined by

the imaginary portion $\varepsilon_2(\omega)$, whereas the real part $\varepsilon_1(\omega)$ describes the compound's polarization upon interaction with an electromagnetic wave. The estimated static $\varepsilon_1(0)$ for $Li_2TlBiCl_6$, $Li_2TlBiBr_6$, and Li_2TlBiI_6 are 2.5 eV, 3.1 eV, and 4.05 eV, accordingly. There is an inverse relation among optical parameters and BG, dictating the Penn's model i.e. $\varepsilon_1(0) \approx 1 + (\frac{\hbar\omega_p}{E_g})^2$ [46].

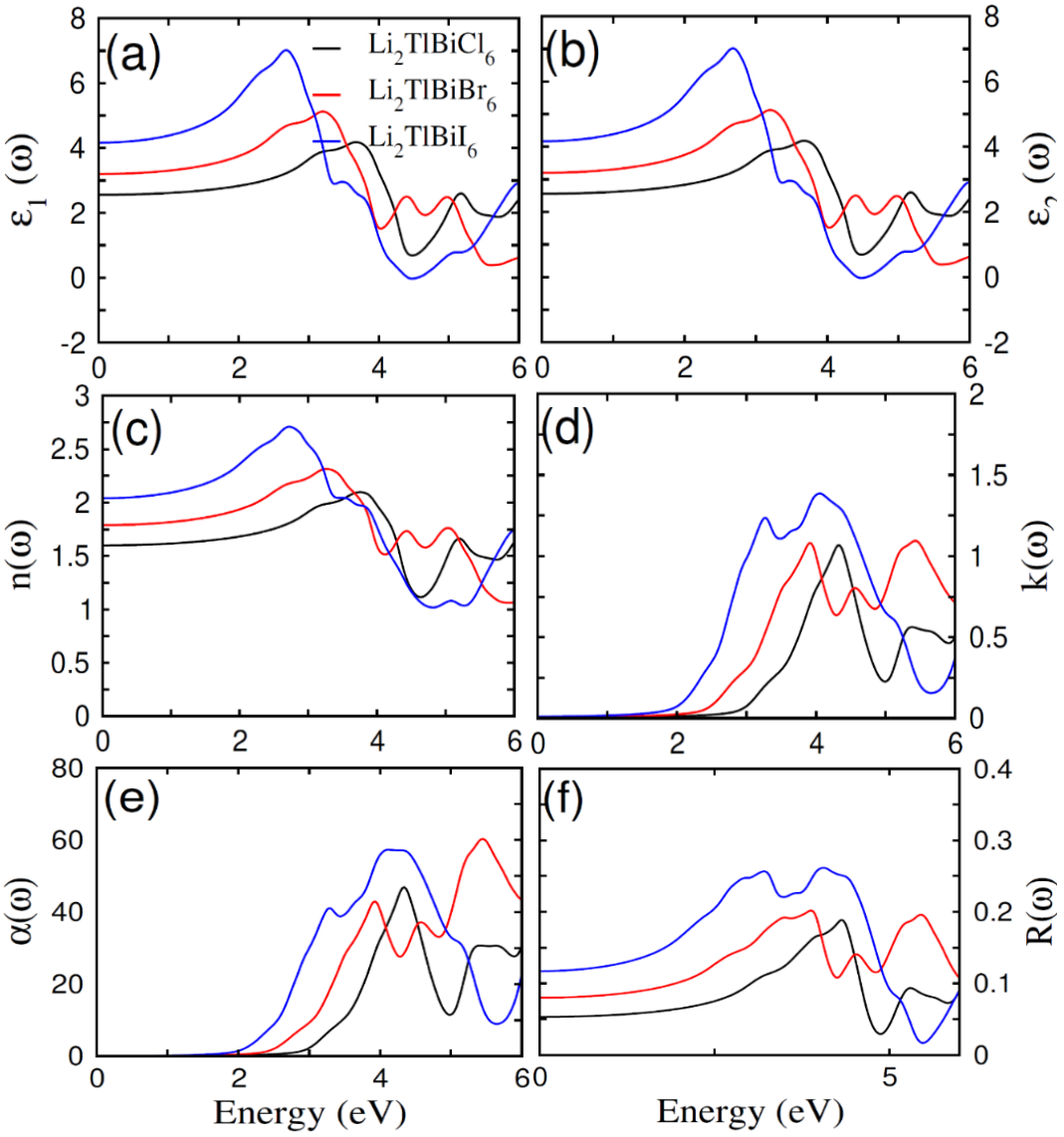

Fig. 5. The estimated (a) real part $\varepsilon_1(\omega)$, (b) imaginary part $\varepsilon_1(\omega)$, (c) refractive index $n(\omega)$, (d) the extinction co-efficient $k(\omega)$, (e) absorption $\alpha(\omega)$, (f) reflectivity $R(\omega)$ of $Li_2TlBiCl_6$, $Li_2TlBiBr_6$ and Li_2TlBiI_6 halides.

The energy absorption evaluation depends on the factor $\varepsilon_2(\omega)$ [47]. Because Br and I ions were substituted for Cl in Li_2TlBiY_6, disintegration took place in threshold absorption energies that varied between 1.0 eV to 2.0 eV. The inter-band shifts are responsible for the elevated estimates of the $\varepsilon_2(\omega)$ (see Fig. 5b), which include 2.6 eV/2.2 eV/1.8 eV for $Li_2TlBiCl_6$/$Li_2TlBiBr_6$/Li_2TlBiI_6. Fig. 5c highlights the refractive index $n(\omega)$ as a function of energy. It affects wavelength, material type, and group velocity.

For $Li_2TlBiCl_6$/$Li_2TlBiBr_6$/Li_2TlBiI_6, the lowest readings of the index of refraction $n(\omega)$ measured at 1.6 eV/1.76 eV/2.1 eV, and the highest figures at 1.55 eV/1.1 eV/1.75 eV. This validates the energy diffusion at diverse wavelengths. According to research by Dahbi et al., doping the molecule $BaTiO_3$ with oxygen groups (S, Se, and Te) modulates its absorption

behavior, which renders it better suited for optoelectronic applications [48]. According to this, Attou et al.'s investigation of semiconductor perovskites, both doped and undoped, revealed that all substituted nanostructures are extremely efficacious and absorbing materials [49].

The formula for the relationship among refractive index and real dielectric coefficient is $n(\omega)_2 - k(\omega)_2 = \varepsilon_1(\omega)$. Figs. 5a and 5c make it evident that this formula meets the requirements of the static dielectric constant and refractive index. Considering optical properties in the visible and infrared energy spectrum, the refractive index in the 1-2 eV region further confirms that all DPs are appropriate for utilization in optical devices. The degree of attenuation is demonstrated by the extinction coefficient, k(ω). Moreover, Figures 5b and 5d manifest how closely its spectral properties analogize $\varepsilon_2(\omega)$. Additionally, the absorption coefficient α(ω), which may be written as $\alpha(\omega)=4\pi k(\omega)/\lambda$ [50], reveals the prominent absorption margins of the interacting energies, and the bandgap is determined in part by how much light the materials absorb. if the bandgap energy is greater than the incident energy, no electronic shift happens from VB to CB. The observed (Fig. 5e) depicted estimated absorption edges of 2.2 eV, 1.8 eV, and 1.5 eV for $Li_2TlBiCl_6$, $Li_2TlBiBr_6$, and Li_2TlBiI_6, completely compatible with the electronic band gaps and fairly congruent with experimental results of related family compounds [51]. On the conclusion, the compounds under investigation are vulnerable in the production of photovoltaic cell devices that operate in visible light [51, 52].

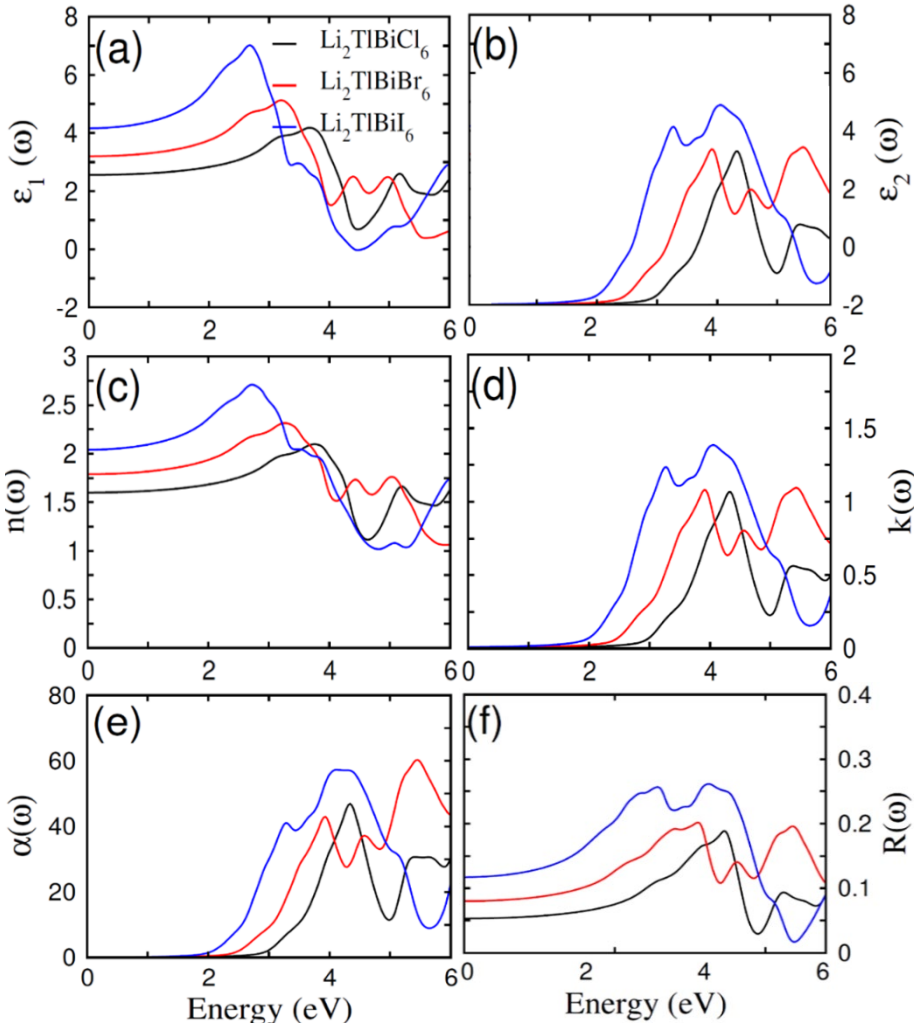

Fig. 5. The calculated (a) real part $\varepsilon_1(\omega)$, (b) imaginary part $\varepsilon_1(\omega)$, (c) refractive index n(ω), (d) the extinction co-efficient k(ω), (e) absorption α(ω), (f) reflectivity R(ω) of $Li_2TlBiCl_6$, $Li_2TlBiBr_6$ and Li_2TlBiI_6 halides.

The material's surface reflectivity is shown by the reflectivity coefficient $R(\omega) = \left|\frac{\sqrt{\varepsilon(\omega)}-1}{\sqrt{\varepsilon(\omega)}+1}\right|^2$ as seen in Fig. 5f [53, 54]. But for $Li_2TlBiCl_6$, $Li_2TlBiBr_6$, and Li2CuBiI_6, the computed value is consistent up to 2 eV before achieving its highest measurements at 4.3 eV (0.08), 3.9 eV (0.12), and 3.5 eV (0.09). A greater part of the incident radiations in radiations in the present study is held by the attenuation. The estimated spectra demonstrate that the optical characteristics in the reported compounds seem unaltered for this factor.

According to Hamideddine et al. [51], applying stress causes energy band in AGeI_2Br (A = Cs, Rb, and K) to widen; yet, no variation in optical characteristics results in an excellent absorption coefficient, confirming the material's potential for use in solar energy technologies. Consequently, the highest absorption in the visible range accompanied by reduced reflection, dispersion, and energy loss supports the use of the reported DPs in the production of photovoltaic cells and optoelectronic appliances.

3.3. Thermoelectric properties

The noteworthy Seebeck coefficient measurement as well as band alongwith indirect trait boosted the worth of the reported double perovskites in thermal oriented applications [55]. A compound's appropriate BG suggests using it in energy-harvesting applications whereas it contributes significantly to electricity production [56]. Thermoelectric compounds have been extensively researched in the last few decades [57, 58]. The BoltzTrap algorithm was employed for the computation of heat conduction constant of Li_2TlBiY_6, excluding phonon participation. The computed transport properties of the compounds are shown in Figs. 6a–f. The electric conductivity is normalized by several parameters, including charge quantity, mobility parameters, and charge carrier density. Electric conductivity and charge carrier concentration have been demonstrated to rise linearly at 300–800K (Fig. 6a). It is known that the ideal temperature for producing enough power for band spliting and form required charges necessary for conductivity is thought to be 300K. Fig. 6a illustrates the concentration of charge carriers and the rise in electrical conduction. By using the final value of σ/τ at 300K for Li2CuBiI_6, a concerning adaptability of charge carriers has been determined, reflecting the relatively tiny BG. When we swap out Cl atoms for Br and I atoms, the BG lessens due to the reciprocal relationship among temperature and electrical conduction.

The experimental relaxation times and semiconductor relaxation times ((10^{-14}s)) for the compounds under investigation have not yet been discovered in this research. As a result, 10^{-14} s is the maximum relaxation time. Fig. 6c shows a plot of k_e vs temperature in this manner. In semiconductor materials, phononic waves are produced by lattice vibrations and carriers that supply heat power for thermal conductivity. The restrictions on the algorithm restrict the calculation only to electrical component of thermal conductivity. Nonetheless, thermal conductivity could be more broadly recognized by applying the Fourier law ($q = - dT/dx$). Q= heat flux, dT/dx = temperature gradient, k_e/τ= coefficient of thermal conductivity. To improve the compounds' thermoelectric productivity, certain electrical and thermal parameters are needed. Li_2TlBiZ_6 is thought to have an approximate thermal conductivity since all of the DPs have significant atomic radii.

At room temperature, S coefficient approaches positive value approaching towards exhibition of the materials under study exhibiting p-type conduction (see Fig. 6b). The S parameter figure escalates by the escalation of temperature up to 400K & then falls down 800K. The heat capacity (Cv) is analyzed between 300K and 800K in temperature. The proportion of the compound's total heat energy to the induced thermal gradient is referred to as Cv [59]. Fig. 6d depicts in the analyzed DPs that the escalation in temperature leads to a rising trend in Cv. For $Li_2TlBiCl_6$, $Li_2TlBiBr_6$, and Li_2TlBiI_6, the specific ambient temperature ranges for Cv are (0.29, 0.35, and 0.25) J mol^{-1} K^{-1}, accordingly. Moreover, Fig. 6e illustrated power factor ($s^2\sigma$) throughout the temperature variation from 300K to 800K. At 300 K, the power factor approaches $0.7\times10^{11}W/K^2ms$, and when the temperature climbs to 800 K, it grows further.

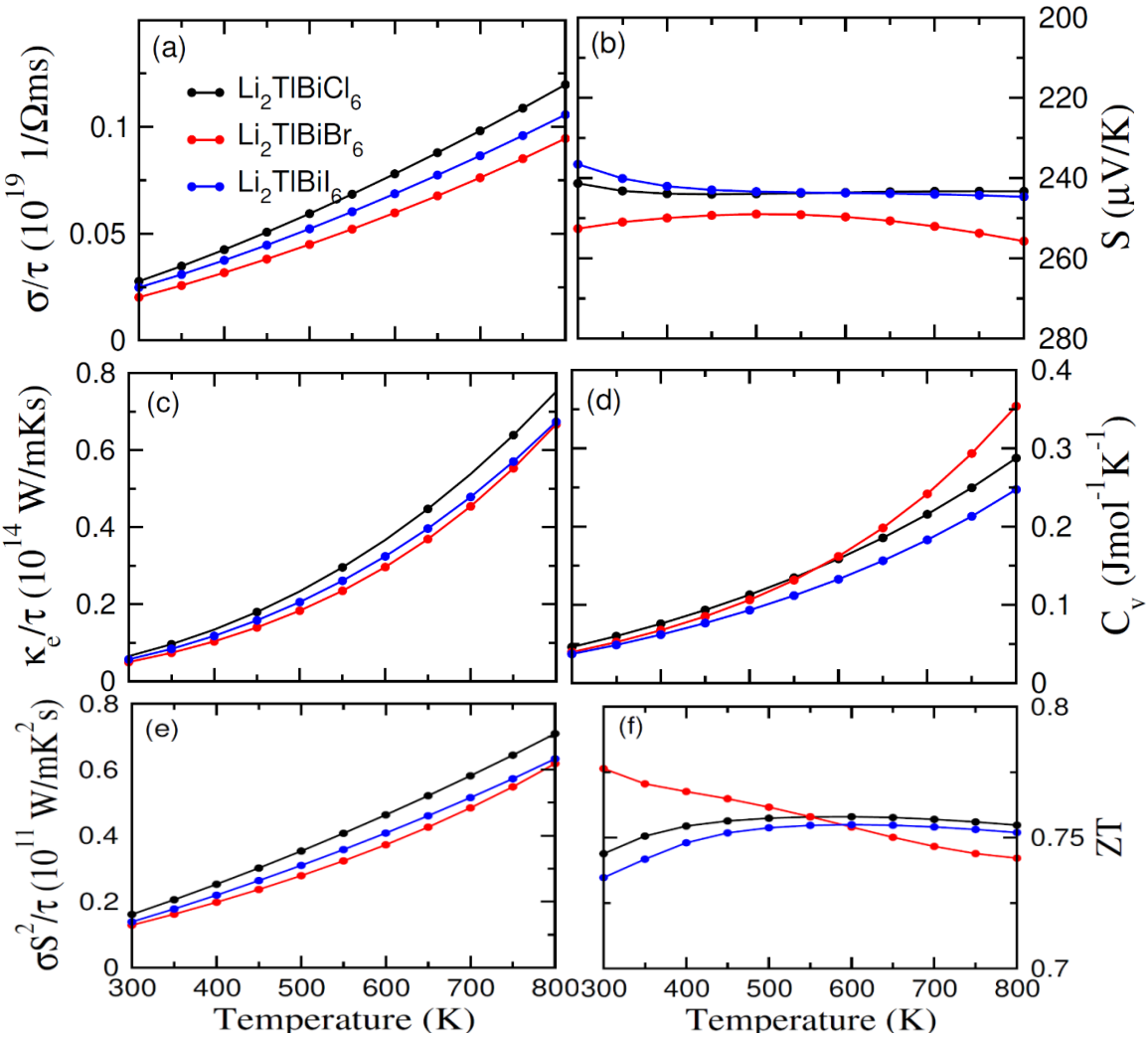

Fig. 6. The estimated (a) electrical conductivity (σ/τ), (b) Seebeck coefficients (S), (c) thermal conductivity (k_e/τ), (d) Specific heat capacity (Cv), (e) power factor and (f) figure of merit against the temperature of $Li_2TlBiCl_6$, $Li_2TlBiBr_6$ and Li_2TlBiI_6 halides.

Besides the Seebeck coefficient, both conduction parameters determine ZT= $\sigma S^2/k$. For double perovskites, the thermal conductivity rises with the S parameter. However, the magnitude of thermal conductivity stays minimal, often for a variety of materials. ZT measurements for Li_2TlBiY_6 are highest at ambient temperature and fall as the temperature rises. On the other hand, the importance of Li_2TlBiI_6 in the development of thermoelectric devices is enhanced despite being at room temperature. Furthermore, as comparable family compounds Ba_2YBiO_6 have better Seebeck coefficients and Figures of Merit, all DPs are optimal for thermoelectric power generation [50].

4. Conclusion

The mechanical, optoelectronic and transport characteristics of DPs Li_2TlBiY_6 are investigated via the DFT-based Wien2k program. The physical stability existence of the studied DPs is demonstrated by the Born stability standards and the negative formation energy H_f. These DPs have direct band gaps (2.8, 2.3, and 1.9 eV, respectively) for photovoltaic devices, making them a great substitution of DPs. Maximum absorbability appears in visual spectra with lowest optical loss indicating all DPs are potentially used for optoelectronic devices. The optimal domain

of transparency as well as polarization can be seen in their index of refraction for the DPs under examination. Additionally, the thermoelectric research shows our compounds' outstanding performance at ambient temperature as well as the possibility of increasing this efficiency to higher temperatures.

Funding

Researchers Supporting Project number (RSPD2024R741), King Saud University

Acknowledgements

The authors would like to thank the Researchers Supporting Project number (RSPD2024R741), King Saud University, Riyadh, Saudi Arabia.

References

[1] A.H. Slavney, T. Hu, A.M. Lindenberg, H.I.A. Karunadasa, J. Am. Chem. Soc. 138 (2016) 2138- 2141; https://doi.org/10.1021/jacs.5b13294

[2] E.T. McClure, M. R. Ball, W. Windl, P.M. Woodward, Chem. Mater. 28 (2016) 1348- 1354; https://doi.org/10.1021/acs.chemmater.5b04231

[3] N. R. Wolf, B.A. Connor, A.H. Slavney, H.I. Karunadasa, Angew. Chemie - Int. Ed. 60 (2021) 16264-16278; https://doi.org/10.1002/anie.202016185

[4] E. Greul, M.L. Petrus, A. Binek, P. Docampo, T. Bein, Highly Stable, J. Mater. Chem. A 5 (2017), 19972-19981; https://doi.org/10.1039/C7TA06816F

[5] M. C. Jung, S. R. Raga, Y. Qi, RSC Advances 6 (2016) 2819; https://doi.org/10.1039/C5RA21291J

[6] S. Galliano, F. Bella, M. Bonomo, G. Viscardi, C. Gerbaldi, Nanomaterials 10 (2020) 1585; https://doi.org/10.3390/nano10081585

[7] E. Pulli, E. Rozzi, F. Bella, Energy Conv Manag 219 (2020) 112982; https://doi.org/10.1016/j.enconman.2020.112982

[8] F. Bella, L. Porcarelli, D. Mantione, C. Gerbaldi, Chem. Sci. 11 (2020) 1485; https://doi.org/10.1039/C9SC05596G

[9] M.A. Bavio, J.E. Tasca, G.G. Acosta, M.F. Ponce, R.O. Fuentes, A. Visintin, J. Solid-State Electrochemistry, 24 (2020) 699-710; https://doi.org/10.1007/s10008-020-04511-7

[10] B. Singh, M. Vogl, S. Wurmehl, S. Aswartham, B. Büchner, P. Kumar, Physical Review Research, 2 (2020) 023162; https://doi.org/10.1103/PhysRevResearch.2.013040

[11] A.C. Ferreira, S. Paofai, A. Létoublon, J. Ollivier, S. Raymond, B. Hehlen, B. Rufflé, S. Cordier, C. Katan, J. Even, P. Bourges, Communications Physics, 3(2020) 1-10; https://doi.org/10.1038/s42005-020-0313-7

[12] M. Cong, B. Yang, F. Hong, T. Zheng, Y. Sang, J. Guo, S. Yang, K. Han, Science Bulletin.65 (2020) 1078-1084; https://doi.org/10.1016/j.scib.2020.03.010

[13] X. Liu, W. Zhao, H. Cui, Y. Xie, Y. Wang, T. Xu, F. Huang, Inorg. Chem. Front. 2(2015) 315-335; https://doi.org/10.1039/C4QI00163J

[14] T. Zhang, H. Li, H. Ban, Q. Sun, Y. Shen, M. Wang, J. Mater. Chem. A, 8 (2020) 4118-4124; https://doi.org/10.1039/C9TA11794F

[15] G. Murtaza, T. Alshahrani, R. M. A. Khalil, Q. Mahmood, T. H. Flemban, H. Althib, A. Laref, J. Solid State Chemistry, 297 (2021)121988; https://doi.org/10.1016/j.jssc.2021.121988

[16] T. Ghrib, A. Rached, E. Algrafy, I. A. Al-nauim, H. Albalawi, M. G. B. Ashiq, B. Ul Haq, Q. Mahmood, Materials Chemistry and Physics, 264 (2021)124435;

https://doi.org/10.1016/j.matchemphys.2021.124435
[17] Q. Mahmood, M. H. Alhossainy, M. S. Rashid, T. H. Flemban, H. Althib, T. Alshahrani, M. Rashid, A. Laref, Materials Science and Engineering: B, 266 (2021)115064; https://doi.org/10.1016/j.mseb.2021.115064
[18] A. Purkayasth, A. T. Mallajosyula, Solar Energy 218 (2021) 251-261; https://doi.org/10.1016/j.solener.2021.01.054
[19] D.A. Chalkias, A. Karavioti, A.N. Kalarakis, E. Stathatosa, Solar Energy 224 (2021) 1017-1027; https://doi.org/10.1016/j.solener.2021.06.074
[20] U. Khan, Y. Zhinong, A.A. Khan, A. Zulfiqar, Q.U. khan, Solar Energy 189 (2019) 421-425; https://doi.org/10.1016/j.solener.2019.06.061
[21] L. Huang, X. Cui, C. Liu, W. Yang, W. Shi, J. Lai, L. Wang, Solar Energy 199 (2020) 826-831; https://doi.org/10.1016/j.solener.2020.02.080
[22] Faddouli, A., H. Labrim, S. Fadili, A. Habchi, B. Hartiti, M. Benaissa, M. Hajji, H. Ez-Zahraouy, E. Ntsoenzok, A. Benyoussef. Renewable Energy 147 (2020) 2077-2090; https://doi.org/10.1016/j.renene.2019.09.130
[23] F. Giustino, H.J. Snaith, Toward lead-free perovskite solar cells. ACS Energy Lett. 1, (2016) 1233-1240; https://doi.org/10.1021/acsenergylett.6b00499
[24] G.X. Zhao, J.H. Yang, Y. Fu, D. Yang, Q. Xu, L. Yu, S.H. Wei, L. Zhang, J. Am. Chem. Soc. 139 (2017) 2630-2638; https://doi.org/10.1021/jacs.6b09645
[25] M.R. Filip, S. Hillman, A.A. Haghighirad, H.J. Naith, F. Giustino, J. Phys. Chem. Lett. 7 (2016) 2579-2585; https://doi.org/10.1021/acs.jpclett.6b01041
[26] W. Shockley, H.J. Queisser, J. Appl. Phys. 32 (1961) 510- 519; https://doi.org/10.1063/1.1736034
[27] X. Huang, S. Huang, P. Biswas, R. Mishra, J. Phys. Chem. C 120, (2016) 28924-28932; https://doi.org/10.1021/acs.jpcc.6b09567
[28]. S. A. Mir, D. C. Gupta, Int. J. Energy Res., 2019, 43, 4783-4796; https://doi.org/10.1002/er.4620
[29] P. Blaha, K. Schwarz, G.K.H. Madsen, D. Kvasnicka, J Luitz, K. Schwarz (Ed.), WIEN2K, "An Augmented Plane Wave, Local Orbitals Program for Calculating Crystal Properties, Techn. Universitat, Vienna, Austria (2001)
[30] J. P. Perdew, K. Burke, M. Ernzerhof, Phys. Rev. Lett., 1996, 77, 3865-3868; https://doi.org/10.1103/PhysRevLett.77.3865
[31] F. Tran, P. Blaha, Phys. Rev. Lett., 102 (2009) 22640; https://doi.org/10.1103/PhysRevLett.102.226401
[32] G.K. Madsen, D.J Singh. BoltzTraP., Comp. Phys. Communi. 175 (2006) 67-71; https://doi.org/10.1016/j.cpc.2006.03.007
[33] H. Rached, Int. J. Quantum Chem., 121(2021) 26647; https://doi.org/10.1002/qua.26647
[34] Y. Rached, M. Caid, D. Rached, H. Rached, Materials Science in Semiconductor Processing, 156 (2023) 107297; https://doi.org/10.1016/j.mssp.2022.107297
[35] S. Al-Qaisi, M.A. Ali, T.A. Alrebdi, T.V. Vu, M. Morsi, B.U. Haq, R. Ahmed, Q. Mahmood, S.A. Tahir, First-principles investigations of Ba2NaIO6 double Phys. 275 (2022), 125237; https://doi.org/10.1016/j.matchemphys.2021.125237
[36] M. Marsman, N. Marzari, U. Nitzsche, L. Nordström, Science 351 (2016) 6280
[37] A. E. Fedorovskiy, N. A. Drigo, M. K. Nazeeruddin, Small Methods 1 (2019) 1900426.
[38] G. Murtaza, Thamraa Alshahrani, R.M. Arif Khalil, Q.Mahmood, Tahani H. Flemban, Hind Althib, A. Laref, J. Solid State Chem. 297 (2021) 121988; https://doi.org/10.1016/j.jssc.2021.121988
[39] Max Born; Kun Huang; M. Lax, Dynamical Theory of Crystal Lattices, Am. J. Phys. 23, 474 (1955); https://doi.org/10.1119/1.1934059
[40] Mohamed Hichem Elahmar, Habib Rached, Djamel Rached, Mater. Chem. Phys. 267 (2021) 124712; https://doi.org/10.1016/j.matchemphys.2021.124712

[41] Caid, M., D. Rached, S. Al-Qaisi, Y. Rached, H. Rached, Solid State Communications 369 (2023): 115216; https://doi.org/10.1016/j.ssc.2023.115216

[42] G.N. Greaves, A.L. Greer, R.S. Lakes, T. Rouxel, Nature materials, 10 (2011) 823-837; https://doi.org/10.1038/nmat3134

[43] I. Kars Durukan, Y. Oztekin Ciftci, Indian Journal of Physics, 95(2021) 2303-2312; https://doi.org/10.1007/s12648-020-01887-0

[44] C. Kaderoglu, G. Surucu, A. Erkisi, Journal of Electronic Materials, 46 (2017) 5827-5836; https://doi.org/10.1007/s11664-017-5600-z

[45] K.C. Bhamu, A. Sonic, J. Sahariya Sol. Energy, 162 (2018) 336-343; https://doi.org/10.1016/j.solener.2018.01.059

[46] D.R. Penn, Phys. Rev., 128 (1962), pp. 2093-2097; https://doi.org/10.1103/PhysRev.128.2093

[47] N.A. Noor, Q. Mahmood, M. Rashid, B.U. Haq, A. Laref, Ceram. Int., 44 (2018) 13750-13756; https://doi.org/10.1016/j.ceramint.2018.04.217

[48] S. Dahbi, N. Tahiri, O. El Bounagui, H. Ez-Zahraouy, Comp. Cond. Mat. 32 (2022) 00728; https://doi.org/10.1016/j.cocom.2022.e00728

[49] L. Attou, Ahmed Al-Shami, Jaber Boujemaâ, Omar Mounkachi, Hamid Ez-Zahraouy, Phys. Scri. 97 (2022) 115808; https://doi.org/10.1088/1402-4896/ac95d8

[50] Al-Qaisi, Samah, Muhammad Mushtaq, Jamila S. Alzahrani, Huda Alkhaldi, Z. A. Alrowaili, Habib Rached, Bakhtiar Ul Haq, Q. Mahmood, M. S. Al-Buriahi, Manal Morsi, Micro and Nanostructures 170 (2022): 207397; https://doi.org/10.1016/j.micrna.2022.207397

[51] I. Hamideddine, H. Jebari, N. Tahiri, O. El Bounagui, H. Ez-Zahraouy, International Journal of Energy Research 46 (2022): 20755-20765; https://doi.org/10.1002/er.8372

[52] N.A. Noor, M. Hassan, M. Rashid, S.M. Alay-e-Abbas, A. Laref, Mater. Res. Bull., 97 (2018), pp. 436-443; https://doi.org/10.1016/j.materresbull.2017.09.039

[53] Y. Sun, Y. Liu, R. Li, Y. Li, S. Bai, Frontiers in Chemistry 10 (2022) 865281; https://doi.org/10.3389/fchem.2022.865281

[54] Q. Mahmood, T. Ghrib, A. Rached, A. Laref, M.A. Kamran, Materials Science in Semiconductor Processing, 112 (2020) 105009; https://doi.org/10.1016/j.mssp.2020.105009

[55] S. Maqsood, G. Murtaza, N. A. Noor, R. Neffati, Sadia Nazir, A. Laref. Journal of Materials Research and Technology 21 (2022) 841-849; https://doi.org/10.1016/j.jmrt.2022.09.073

[56] J. Kangsabanik, V. Sugathan, A. Yadav, A. Yella, and A. Alam, Physical Review Materials, 2 (2018) 055401; https://doi.org/10.1103/PhysRevMaterials.2.055401

[57] H. Haque, M.A. Hossain, 2018, Potential thermoelectric materials; https://doi.org/10.1016/j.jallcom.2018.03.137

[58] K. Biswas, J. He, I.D. Blum, C.I. Wu, T.P. Hogan, D.N. Seidman, V. P Dravid, M.G. Kanatzidis, Nature, 489 (2012) 414; https://doi.org/10.1038/nature11439

[59]. P. Ruleovaa, C. Drasar, P. Lostak, C.P. Li, S. Ballikaya, C. Uher Mater. Chem. Phys., 119 (2010), p. 2991; https://doi.org/10.1016/j.matchemphys.2009.08.067